Arabian Journal of Chemistry (2020) 13, 3934–3945

King Saud University

Arabian Journal of Chemistry

www.ksu.edu.sa
www.sciencedirect.com

ORIGINAL ARTICLE

Vertical copper oxide nanowire arrays attached three-dimensional macroporous framework as a self-supported sensor for sensitive hydrogen peroxide detection

D.M. Nguyen [a,1], H.N. Bich [b,1], P.D. Hai Anh [c,d], P.H. Ai-Le [e], Q.B. Bui [f,*]

[a] *Institute of Research and Development, Duy Tan University, Da Nang 550000, Viet Nam*
[b] *Center of Excellence for Green Energy and Environmental Nanomaterials, Nguyen Tat Thanh University, Ho Chi Minh City, Viet Nam*
[c] *Automotive Engineering and Technology, Sao Do University, Hai Duong, Viet Nam*
[d] *SYMME, Université Savoie Mont Blanc, FR-74000 Annecy, France*
[e] *Faculty of Chemical Engineering-Industrial University of Ho Chi Minh City, Ho Chi Minh City, Viet Nam*
[f] *Sustainable Developments in Civil Engineering Research Group, Faculty of Civil Engineering, Ton Duc Thang University, Ho Chi Minh City, Viet Nam*

Received 25 January 2019; accepted 8 April 2019
Available online 13 April 2019

KEYWORDS

Copper oxide nanowires;
Three-dimensional substrate;
Electrocatalyst;
Hydrogen peroxide detection;
Self-supported sensors

Abstract A hierarchical nanostructure consisting of uniform copper oxide nanowires vertically grown on three-dimensional copper framework (CuO NWs/3D-Cu foam) was prepared by a two-step synthetic process. The uniform CuO NWs anchored onto the 3D foam exhibited outstanding electrocatalytic activity towards hydrogen peroxide reduction due to the unique one-dimensional direction with its excellent catalytic activity and large surface area of 3D substrate, which enhanced electroactive sites and charge conductivity. As a result, a wide linear detection range of 1 μM–1 mM, good sensitivity of 8.87 μA/(mM ṡ cm^2), low detection limit of 0.98 μM, and rapid response time of 5 s to hydrogen peroxide were achieved under a working potential of −0.4 V in phosphate buffer solution (pH of 7.4). In addition, the CuO NWs/3D-Cu foam material showed excellent selectivity to hydrogen peroxide and good resistance against poisonous interferents, including ascorbic acid, dopamine, urea, uric acid, and potassium chloride. Furthermore, the CuO NWs/3D-Cu foam presented good reproducibility, stability, and accurate detection for

* Corresponding author.
E-mail address: buiquocbao@tdtu.edu.vn (Q.B. Bui).
[1] These authors have equal contribution.
Peer review under responsibility of King Saud University.

Production and hosting by Elsevier

https://doi.org/10.1016/j.arabjc.2019.04.002

hydrogen peroxide in real sample; therefore, it may be considered to be a potential free-standing hydrogen peroxide sensor in practical analysis applications.

1. Introduction

Hydrogen peroxide (H_2O_2) is one of the important substances displaying critical role in biological process and various application, such as pharmacy, food industry, manufacturing processes, environmental protection, and enzymatic reactions (Marinho et al., 2014; Li et al., 2012). Some neurodegenerative diseases, including Alzheimer's and Parkinson's are also associated with the high content of H_2O_2, which is generated by neuronal mitochondria in brain (Milton, 2004; Shichiri, 2014). In this context, the interaction between H_2O_2 with iron and copper to produce highly toxic reactive oxygen species may offer a mechanism of the oxidative stress, thereby leading to Alzheimer's and Parkinson's disease. Therefore, the sensitive and accurate detection of H_2O_2 concentration has been an important requirement in health care as well as industrial purposes. Great attention has focused on H_2O_2 detection via different methods, such as spectrometry, chromatography, titration, and chemiluminescence (Shiang et al., 2009; Gimeno et al., 2015; Tarvin et al., 2011; Ryoo et al., 2017); however, these approaches have some limitations, such as complicated procedure, high costs, and long analysis time. To address these issues, the electrochemical approach has recently been emerging as the spotlight with low cost, high sensitivity, quick response, low limit of detection (LOD), and good selectivity towards H_2O_2 sensing (Chen et al., 2012, 2013). For improving the performance of working electrode via electrochemical analysis, the modification of the electrode's surface by a catalytic nanomaterial is highly necessary (Liu, 2017; Shao et al., 2010). However, the use of a polymer to attach nanomaterial on electrode is commonly required and it makes sensor face some weaknesses, such as reduced conductivity and low sensitivity due to prohibition of electron transport, generation of additional undesirable interfaces, and decrease in the electroactive sites of electrocatalyst. In addition, the use of enzyme to increase selectivity and sensitivity of sensor also leads to some disadvantages, including complex immobilization procedure, instability, and high cost (Toghill, 2014). Therefore, it is really necessary to develop a novel electrochemical sensor without the use of polymer binder and enzyme but high sensitivity, facile operation, good stability, and high reproducibility for H_2O_2 detection.

Recently, various metal-based nanocatalysts have been studied to prepare non-enzymatic H_2O_2 detection, including precious metal-based catalysts (Evans et al., 2002; Li et al., 2010, 2014) and nonprecious metal-base catalysts (Xu et al., 2010; Batchelor-McAuley et al., 2008). The precious metal-based catalysts are high catalytic activity; however, the expensiveness significantly limits the extension of their real applications. Recently, nonprecious metal-based nanocatalysts have attract researchers' attention as the alternates due to their high catalytic activity, abundant, low cost, thereby being competitive in commercial applications. As demonstrated by previous reports, the redox reactions between H_2O_2 with nanocatalysts mainly appear at the surface of electrode (Thetford et al., 2010; Xing et al., 2018; Plauck et al., 2016); therefore, more exposed electroactive sites of catalyst will be crucial for a high-performance H_2O_2 sensor. Agreed with this, nanoscale transition metal catalysts applied for H_2O_2 determination should possess high surface area and open geometry to support the adsorption of reactant and charge/mass transfer between catalyst and electrolyte at the interfacial region. In this regard, some common wet chemical synthesis approaches, such as chemical reduction, solvothermal reaction, and hydrothermal reaction have usually been used to prepare different unique nanostructures of the metal oxide catalysts, including nanoparticles, nanowires, and nanorods (Wang et al., 2015; Al-Hardan et al., 2016; Erande and Late, 2016). However, they often produce big size of metal catalysts with agglomeration/aggregation phenomenon and abundant impurities, thereby significantly reducing activity of final products (Zhao et al., 2009). To address these drawbacks, fabricating electrode in which active electrocatalyst directly growing on a large surface area of a conducting substrate is a favorite approach. Recently, numerous Cu-based nanoarchitectures, including nanoparticles, nanorods, nanocubes, nanoneedles, and nanowires, have been studied for construction of some electrochemical sensors (Etefagh et al., 2013). These Cu-based electrocatalysts not only exhibit cost effectiveness, highly catalytic activity, and great electrical conductivity but also well resist the poison of different interferents in the electrolyte. Especially, one-dimensional (1D) Cu-based nanowires have been stated to be highly sensitive for sensing applications due to their outstanding charge transfer along 1D direction (Yang et al., 2017; Sun et al., 2015). Therefore, the direct growth of 1D Cu-based nanowires on a large area 3D substrate is expected to not only expose more electroactive sites and improve conductivity but also enhance stability and durability for long-term use.

In this work, we fabricated a hybrid based on 1D CuO NWs supported 3D-Cu foam via a two-step synthetic approach. The CuO NWs/3D-Cu foam hybrid has been used as a nonenzymatic binder-free and free-standing sensor towards H_2O_2 detection. It showed charming sensitivity, quick amperometric response, admirable selectivity, and wide detection range due to the superior catalytic activity of CuO NWs and fast electron transfer ability. The good reproducibility and long-term stability of the material are also contributed to the high interaction between CuO NWs and 3D Cu foam.

2. Experimental section

2.1. Chemicals

Ammonium persulfate ($(NH_4)_2S_2O_8$, 98%), hydrogen peroxide (H_2O_2, 30%), dopamine hydrochloride ($(HO)_2C_6H_3CH_2CH_2NH_2{\cdot}HCl$, 99%), uric acid ($C_5H_4N_4O_3$, 99%), ascorbic acid ($C_6H_8O_6$, 99%), sodium phosphate dibasic anhydrous

(Na_2HPO_4, 99%), sodium phosphate monobasic (NaH_2PO_4, 99%), urea (CH_4N_2O, 98%), acetone (CH_3CHO, 99.9%), ethanol (C_2H_5OH, 99.8%), acetic acid (CH_3COOH, 99.8%), and potassium chloride (KCl, 99%), sodium hydroxide (NaOH, 99), and copper foam were purchased from Sigma-Aldrich Chemicals Co. (USA).

2.2. Synthesis of CuOH NWs/3D-Cu foam

The copper foam with the size of 2 cm × 4 cm was firstly cleaned by acetic acid (99.8%), acetone (99.9%), ethanol (99.8%), and pure water for 15 min each to remove the surface oxides and impurities. After that, the cleaned Cu foam was immersed in 50 ml water containing 1.5 g $(NH_4)_2S_2O_8$ and 5.0 g NaOH under magnetic stirring at room temperature for 20 min. Finally, the 3D-Cu foam with the growth of CuOH NWs was collected and rinsed with water until pH = 7 followed by drying under nitrogen flow at room temperature.

2.3. Synthesis of CuO NWs/3D-Cu foam

The resulting CuOH NWs/3D-Cu foam was placed in a quartz boat, which was annealed at 200 °C at a heating rate of 5 °C min^{-1} in air environment for 90 min. After that, the sample was naturally cooled down to room temperature and was collected for characterizations (Fig. 1).

2.4. Material characterization

The morphology of the materials was studied by scanning electron microscope (SEM) JSM 6600 (JEOL Co., Japan) and transmission electron microscope (TEM) JEM-1400 Philips microscope (JEOL Co., Japan). The chemical states of the materials were evaluated Escalab 250Xi X-ray photoelectron spectrometer (Thermo Fisher Scientific Inc., USA). X-ray diffraction (XRD) technique was applied to investigate crystalline structure of the materials via a D8 Advance diffractometer (Bruker Co., Germany) with CuKα radiation (wavelength of 1.54 Å) in a 2θ range of 5–90°. The surface area of the materials was estimated on an SA-9600 Series (HORIBA Co., Japan).

For electrochemical detection of H_2O_2, a ZIVE SP2 2Amp electrochemical workstation (WonATech Co., Ltd., Korea) combining with a three-electrode cell system was applied. The Ag/AgCl reference electrode with 3 M KCl solution as reference electrolyte and Pt wire counter electrode (with length of 5 cm, diameter of 0.5 mm, and surface area of 0.7 cm^2) were used. The CuO NWs/3D-Cu foam (1 cm × 1 cm) was hold in a metallic clamp and was directly used as working electrode. The charge transfer ability of the working electrode was investigated by electrochemical impedance spectroscopy (EIS) in N_2-saturated 0.1 M PBS solution. The catalytic activity of the working electrode towards H_2O_2 reduction was studied using cyclic voltammetry (CV) and amperometry (i-t) in 0.1 M PBS solution. The amperometric measurements were carried out by successive addition of H_2O_2 concentrations into a stirring 0.1 M PBS solution at an applied potential of −0.4 V, and then steady state of current response for each addition was noted. All the electrochemical experiments were conducted at room temperature of 25 ± 1 °C.

3. Result and discussion

Fig. 2 shows SEM images of the bare 3D-Cu foam, CuOH NWs/3D-Cu foam, and CuO NWs/3D-Cu foam hybrid

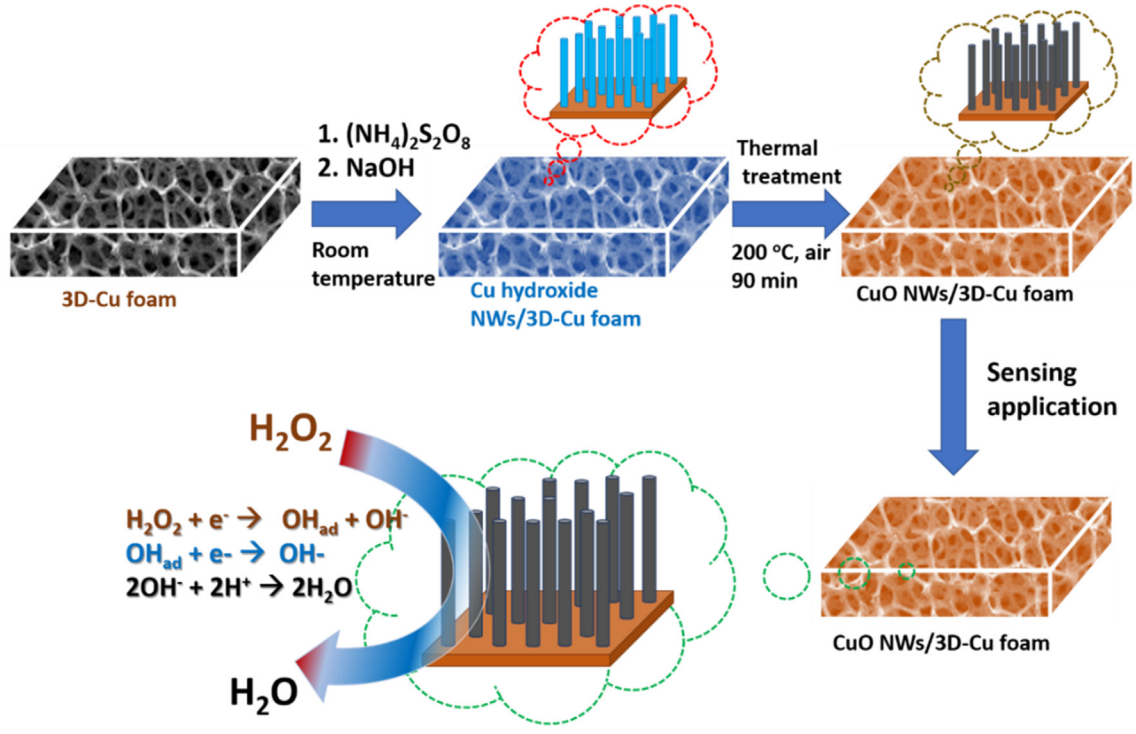

Fig. 1 Schematic illustration for CuO NWs/3D-Cu foam preparation.

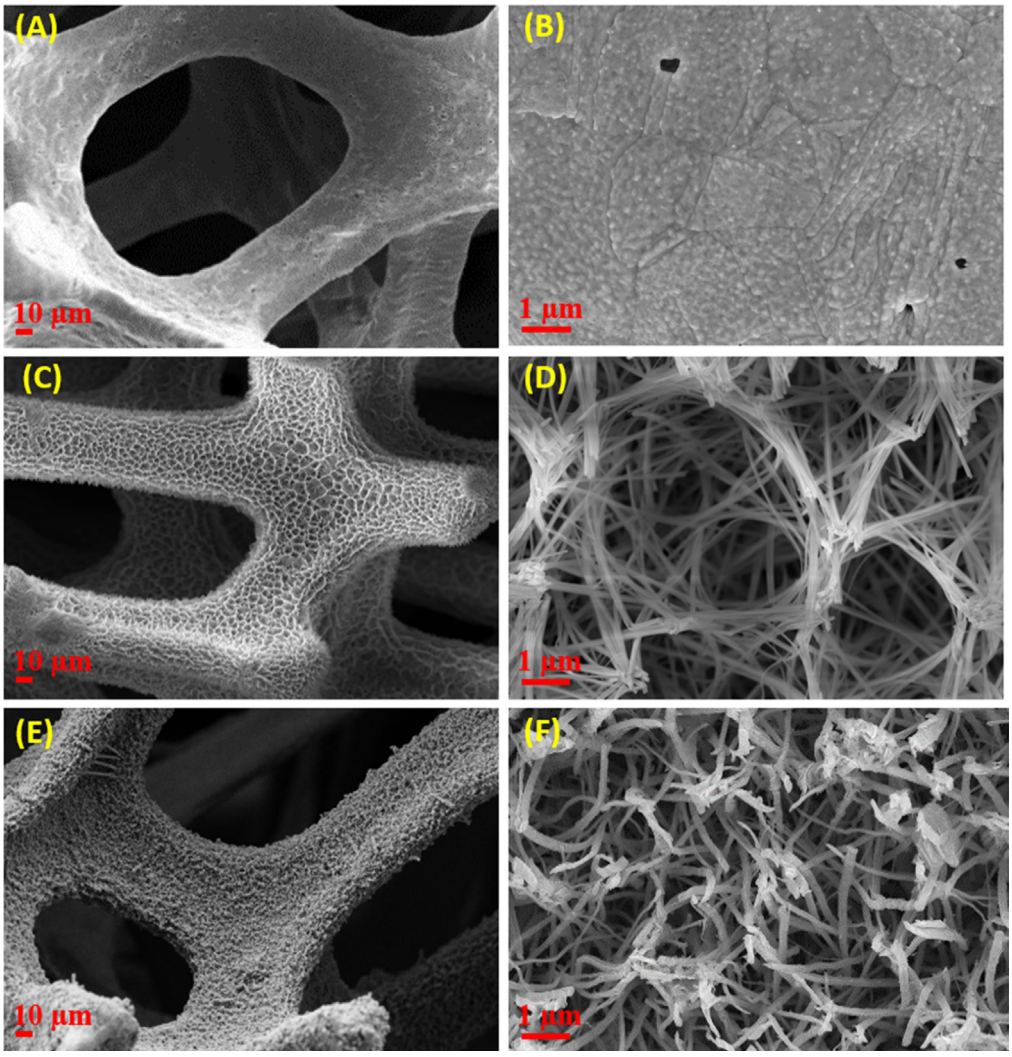

Fig. 2 FE-SEM images at different magnifications of (A and B) bare 3D-Cu foam, (C and D) CuOH NWs/3D-Cu foam, and (E and F) CuO NWs/3D-Cu foam hybrid.

materials. From the top view of the SEM images in Fig. 2A and B, the smooth surface of the bare-3D-Cu foam can be observed. Meanwhile, the low magnification SEM image in Fig. 2C shows the compact CuOH NWs uniformly cover over the 3D-Cu surface. Besides, these NWs are also roughly aligned perpendicular to the surface of the 3D-Cu foam. The high magnification SEM image indicates that the CuOH NWs with an average diameter of 200 nm and length of several ten μm possess smooth surface (Fig. 2D). After a thermal treatment process at 200 °C, the CuOH NWs were completely converted to CuO NWs. The low-magnification SEM image of the CuO NWs/3D-Cu foam is similar to that of the as-prepared CuOH NWs/3D-Cu foam (Fig. 2E). However, the magnified image clearly indicates the significantly rough surface of the CuO NWs, which appear with bending and flexible states to well form interconnected architecture (Fig. 2F), thereby expecting to enhance surface area and conductivity of the material.

Morphology of the CuO NWs/3D-Cu foam hybrid was further investigated by TEM analysis. Fig. 3A shows low-magnification TEM image of the CuO NWs, which have diameter of around 200 nm along with good uniformity, in agreement with the SEM analysis. The high magnification TEM image of a typical NW confirms the noticeable roughness of its surface (Fig. 3C and D), which is suggested to be consistent with the presence of significant crystal defects such as edge dislocations, suggesting to be favoring for electrochemical reactions. The high-resolution TEM image clearly indicates a fringe spacing of 0.23 nm, which well matches to the d(1 1 1) crystal plane in CuO nanostructures (Fig. 3D) (Chandra Rath et al., 2016). The formation of the CuO NWs was further confirmed by scanning TEM (Fig. 3E) and its corresponding EDS color mapping analysis. According to the EDS color mapping result, it can be seen the uniform distribution of Cu and O element over structure of the surveyed CuO NW, firmly informing the composition of the obtained material is consistent with the formation of CuO nanostructures (Fig. 3F and G).

The crystalline features of the CuO NWs on 3D-Cu foam were investigated in Fig. 4A. It can be seen a typical XRD pattern for the synthesized CuO NWs, which matches the single CuO phase under a monoclinic construction (JCPDS 72-0629) (Chen et al., 2012; Jia et al., 2016). In this context, a list

of peaks occurring at 2θ of 32.29, 36.4, 38.61, 48.74, 53.22, 58.1, 61.37, 66.29, 67.82, and 73.44° are associated to d (1 1 0), d(−1 1 1), d(1 1 1), d(−2 0 2), d(0 2 0), d(2 0 2), d (−1 1 3), d(0 2 2), d(1 1 3), and d(3 1 1) crystal planes of the CuO phase, respectively. In addition to some weak peaks at 2θ of 43.29, 50.48, and 74.91°, relating to d(1 1 1), d(2 0 0), and d(2 2 0) crystal planes from Cu metal phase, there is no visible peaks of other contaminations discovered in the XRD pattern, demonstrating the good quality of the synthesized CuO NWs material. More detailed information of the electronic states and chemical composition of the CuO NWs on 3D-Cu foam material was studied by XPS analysis. The surveyed XPS spectrum clearly shows the available binding energies for Cu2p and O1s at 933 and 531 eV, respectively (Fig. 4B) (Jin et al., 2017). As seen in Fig. 4C, the high resolution Cu2p spectrum exhibits two peaks of Cu^{2+}2p3/2 (934 eV) and Cu^{2+}2p1/2 (954.1 eV), along with two satellite peaks at approximately 942.7 and 962.5 eV that are assigned to Cu^{2+} state in CuO (Kuang et al., 2015). In addition, the chemical state of Cu(0) is also confirmed by two peaks observed at 932.5 and 952.3 eV (Singh et al., 2016; Iivonen et al., 2016). Fig. 4D displays the high resolution O1s spectrum, which can be deconvoluted into four components at binding energies of 829.2, 529.9, 531.2, and 532.2 eV, relating to lattice oxygen of Cu_2O (O1), CuO (O2), oxygen vacancy (O3), and adsorbed oxygen (O4), respectively (Wang et al., 2015). The impressive strong intensity and large area of peaks belonging to CuO phase suggest the successful formation of such nanostructure in NWs.

Fig. 4E presents the nitrogen adsorption-desorption isotherms of the CuO NWs/3D-Cu foam hybrid. The isotherms exhibit a combination of type-II and type-IV, implying macroporous and mesoporous features of the synthesized material (ALOthman, 2012). The surface area of the CuO NWs/3D-Cu is found to be 5.5 $m^2 \cdot g^{-1}$. Furthermore, the mesoporous characteristics of the CuO NWs was proven in Fig. 4F, which shows that the pore size distribution is mainly located in the range of 2–20 nm. The big surface area, the mesoporous properties, and the large pore volume of the CuO NWs/3D-Cu foam is highly expected to enhance the catalytic behavior through offering more electroactive centers to catalyze the reduction process of H_2O_2 (Liu et al., 2007).

EIS is a valuable technique to investigate charge transfer ability at the interface region between the electrode material and electrolyte. Fig. 5 displays the EIS results with the Nyquist plots for bare 3D-Cu foam, CuOH NWs/3D-Cu foam, and CuO NWs/3D-Cu foam electrode. The simulated results exhibit that the values of charge transfer resistance for these electrodes rises in the order of bare 3D-Cu foam (12 Ω) = CuO NWs/3D-Cu foam (13.5 Ω) < CuOH NWs/3D-Cu foam (17 Ω). It can be seen that after growing CuOH NWs on surface of the 3D-Cu foam, the R_{ct} value significantly increases owing to the CuOH NWs deterring in the possibility for interfacial charge transfer. The CuO NWs/3D-Cu foam electrode

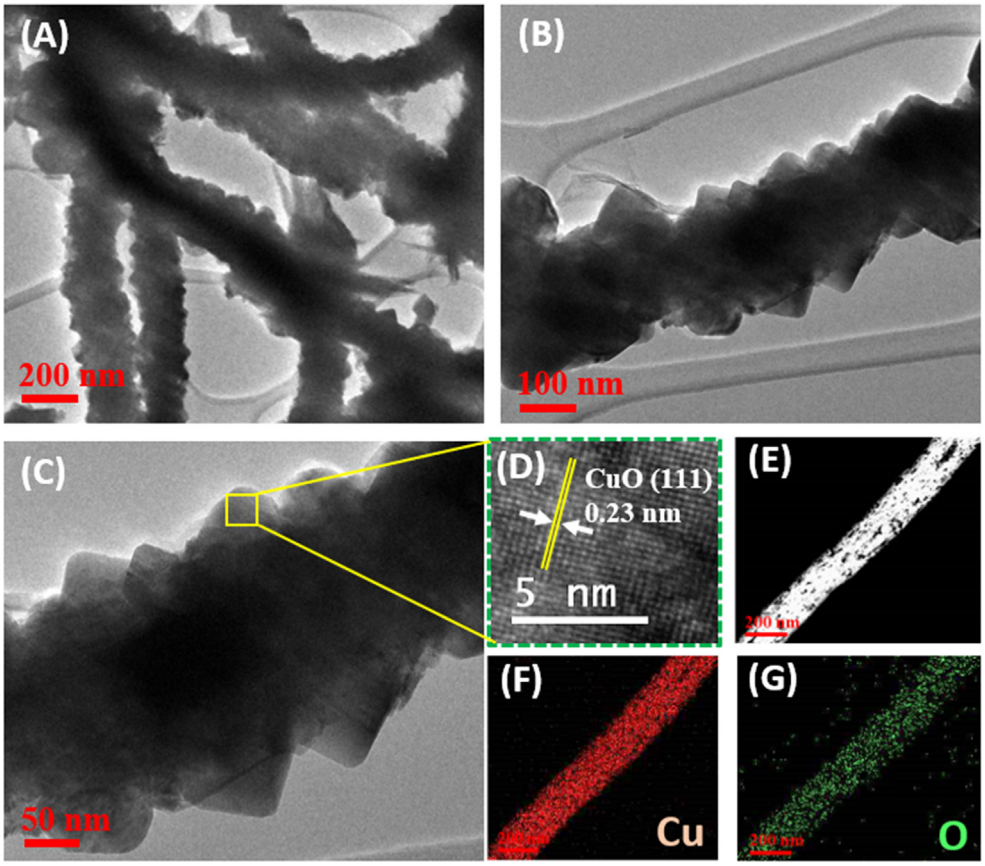

Fig. 3 (A–C) TEM images of the CuO NWs on 3D-Cu foam; (D) HR-TEM image of the CuO NW; (E) Scanning TEM image of the CuO NW and the corresponding EDS color mapping of (F) Cu and (G) O element.

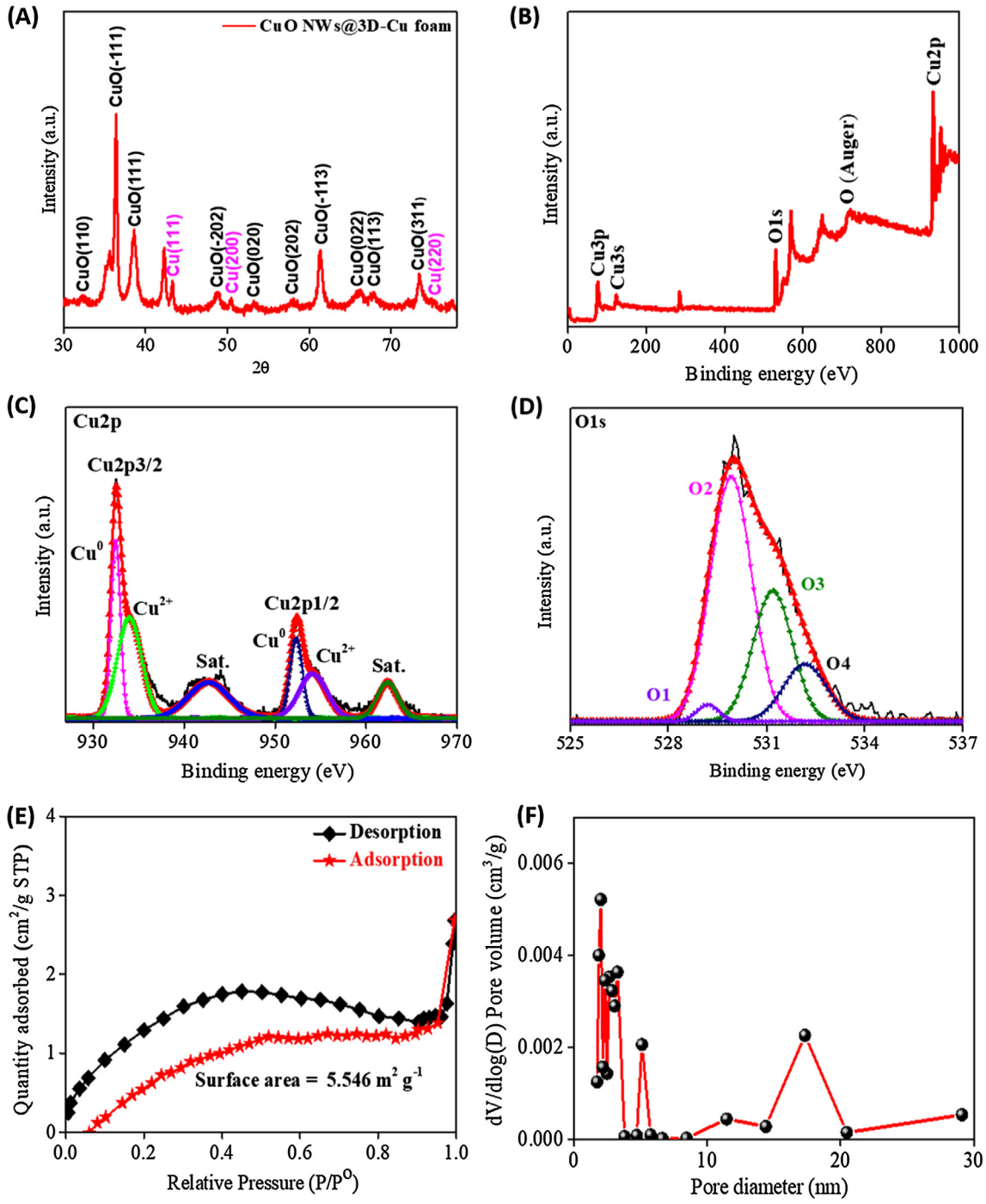

Fig. 4 (A) XRD spectrum and (B) The surveyed XPS spectrum of the CuO NWs/3D-Cu foam; (C) High resolution XPS spectrum of Cu2p in CuO NWs; (D) High resolution XPS spectrum of O1s in CuO NWs; (E) Nitrogen adsorption-desorption isotherms of the CuO NWs/3D-Cu foam; (F) Pore distribution of the CuO NWs/3D-Cu foam.

has smaller semicircle diameter consistent with a lower electron-transfer resistance as compared to the CuOH NWs/3D-Cu foam electrode. This is due to the better conductivity of CuO than that of CuOH structure along with the synergistic effect of 1D CuO NWs and 3D-Cu foam.

The electrocatalytic behavior of the bare 3D-Cu foam, CuOH NWs/3D-Cu foam, and CuO NWs/3D-Cu foam hybrid was investigated in 0.1 M N_2-saturated PBS solution with and without 1 mM H_2O_2 at a scan rate of 50 mV/s. It can be seen that these electrodes show the change of cathodic current density relating to H_2O_2 reduction in the potential range of −0.6 to 0 V (Fig. 6A–C) (Muralidharan, 2015). However, the background current density of the bare 3D-Cu foam is much smaller than those of the CuOH NWs/3D-Cu foam and CuO

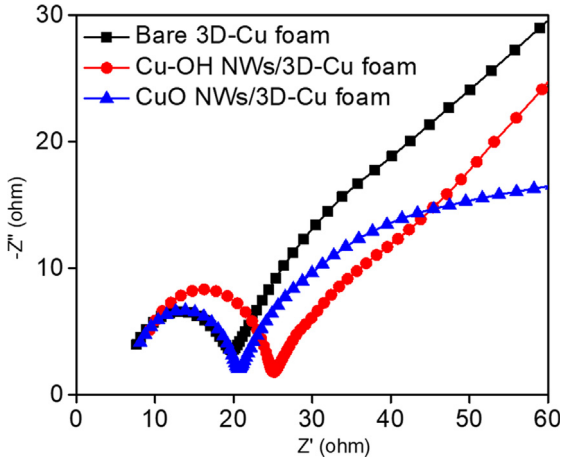

Fig. 5 The EIS results of different electrode materials in 0.1 M PBS solution in the frequency range from 10^5 to 10^{-2}.

NWs/3D-Cu foam; therefore, its response towards to H_2O_2 reduction is much weaker than two other electrodes. The growth of abundant Cu-based NWs on 3D-Cu foam generated more active surface area to produce better catalytic behavior for H_2O_2 detection. In particular, when 1 mM H_2O_2 is added to the reaction system with the presence of CuO NWs/3D-Cu foam electrode, a fast increase in current density and the appearance of an apparent shoulder peak at about −0.4 V are observed, due to effective reduction of H_2O_2 on the surface of CuO NWs (Fig. 6D). The possible reduction mechanism for H_2O_2 at CuO NWs/3D-Cu foam electrode in PBS media can be illustrated by the following steps (Patra and Munichandraiah, 2009):

$$H_2O_2 + e^- \rightarrow OH_{ad} + OH^-$$

$$OH_{ad} + e^- \rightarrow OH^-$$

$$2OH^- + 2H^+ \rightarrow 2H_2O$$

To survey the kinetic of H_2O_2 reduction on surface of the CuO NWs-3D-Cu foam electrode, the CV was measured at different potential scan rates from 15 to 100 mV/s (Fig. 6E). It can be seen that the current response increases with the increase of the scan rate. In this regard, a fitting curve based on current density versus square root of the scan rate displays good linearity (Fig. 6F), demonstrating that the reduction of H_2O_2 at the surface of the CuO NWs/3D-Cu foam is a diffusion controlled process (Nasirizadeh et al., 2016). The noteworthy electrocatalytic performance of the CuO NWs/3D-Cu foam hybrid may be resulted from the enhanced electroactive sites of 1D direction and outstanding catalytic behavior of the CuO NWs, which can expose more electroactive surface area to promote adsorb reactant molecules onto their surface and activate them for decomposition process (Li et al., 2015). In addition, the absence of binder usage also leads to rapid charge transfer (Zhang et al., 2018), thereby creating high current response of electrode towards H_2O_2 reduction reaction.

The effect of different applied potentials on amperometric sensing ability of the CuO NWs/3D-Cu foam electrode was

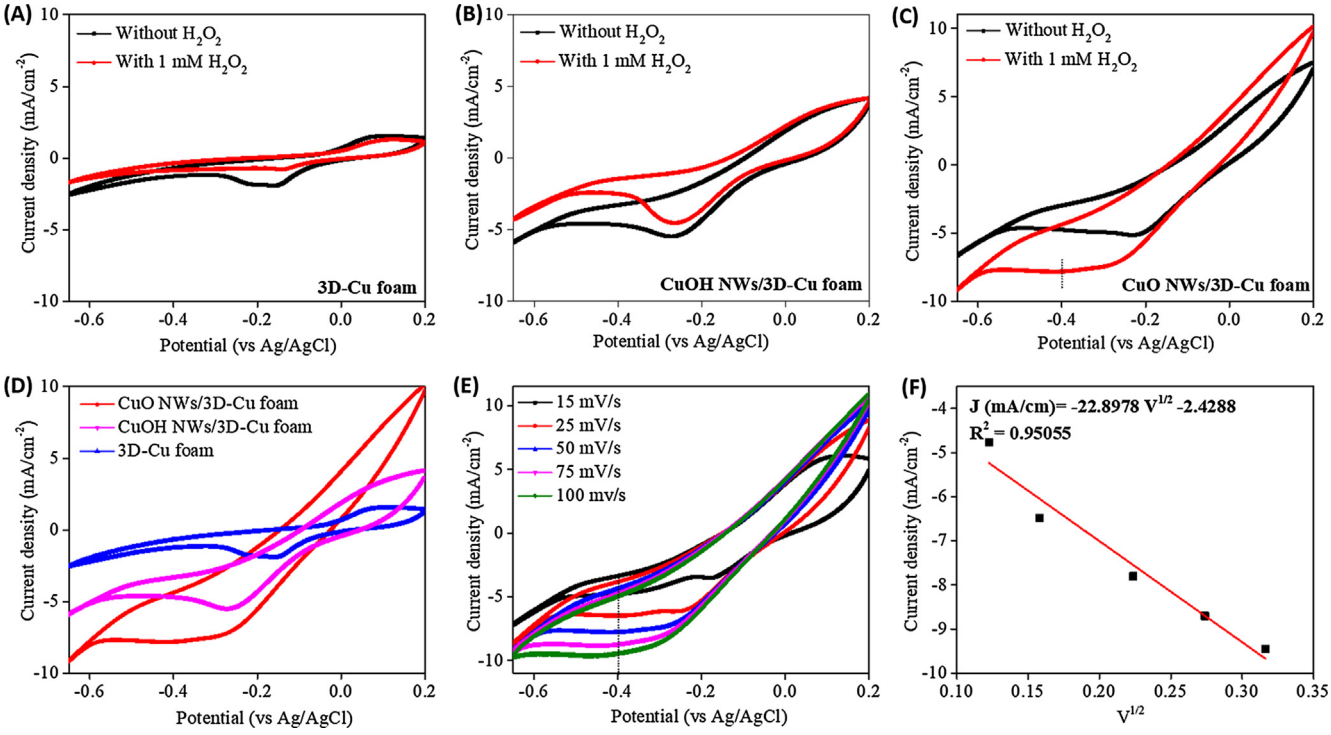

Fig. 6 Cyclic voltammograms of (A) the bare 3D Cu-foam, (B) CuOH NWs/3D-Cu foam, and (C) CuO NWs/3D-Cu foam without and with the presence of 1 mM H_2O_2; (D) Comparison of cyclic voltammograms for different materials; (E) Cyclic voltammograms of the CuO NWs/3D-Cu foam with the presence of 1 mM H_2O_2 at different scan rates, (F) The fitting curve based on current density vs square root of the scan rate.

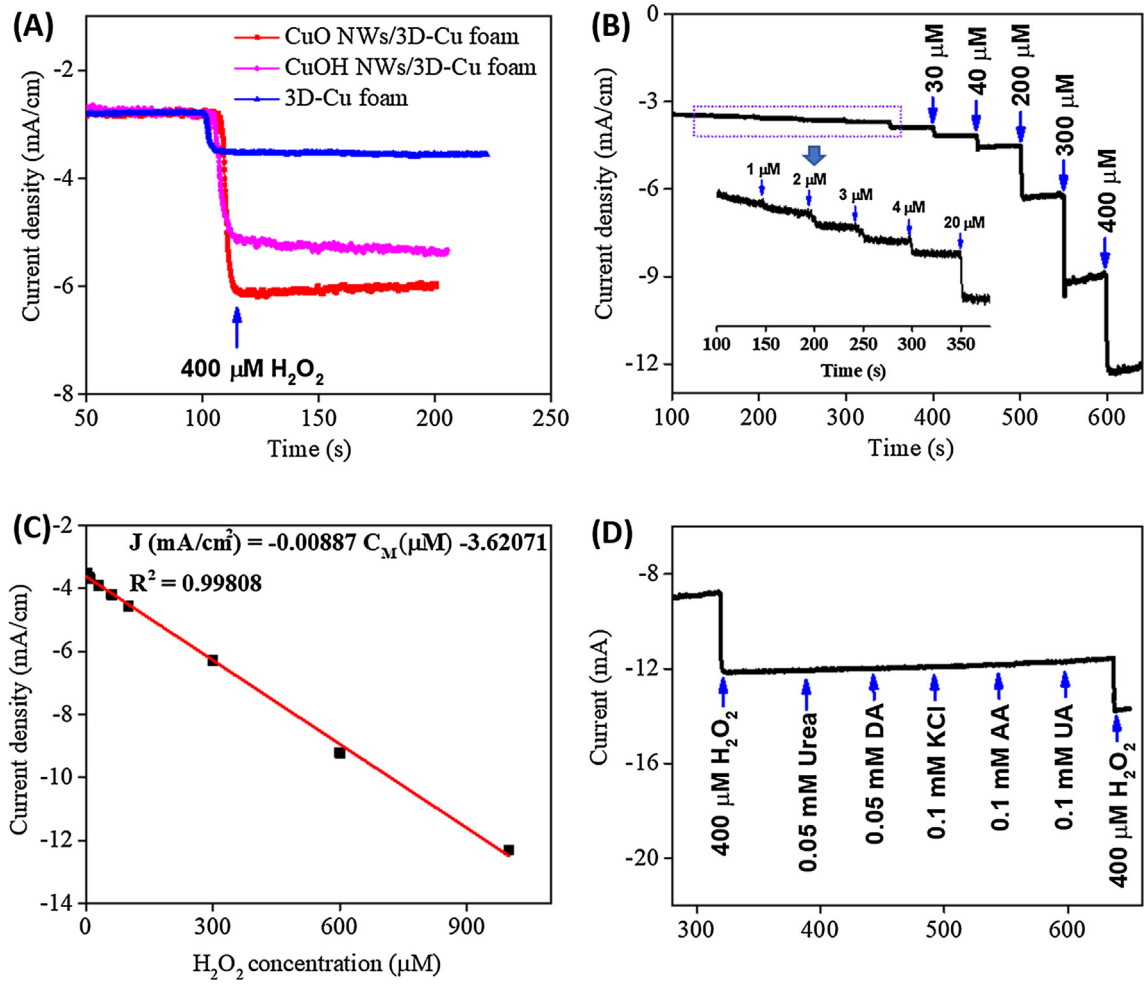

Fig. 7 (A) Amperometry measurements of different materials at an applied potential of −0.4 V in 0.1 M PBS solution with the addition of 0.4 mM H_2O_2; (B) Amperometry response of the CuO NWs/3D-Cu foam electrode at an applied potential of −0.4 V in 0.1 M PBS solution with the addition of different H_2O_2 concentrations; (C) The fitting curve based on amperometry current response vs H_2O_2 concentration; (D) The selectivity of the CuO NWs/3D-Cu foam electrode.

Table 1 Comparison the catalytic performance of the CuO NWs/3D-Cu foam electrode with recent reports for H_2O_2 detection.

Materials	Linear detection range (μM)	LOD (μM)	Sensitivity ($\mu A \dot{s} \mu M^{-1} \dot{s} cm^{-2}$)	References
CuO/GCE	5–180	1.6	0.0086	Zhang et al. (2011)
Hb–kieselgubr film	5–300	2.1	–	Wang et al. (2002)
Poly(indole-*co*-thiophene)/Fe_3O_4	2–350	0.54	–	Baghayeri et al. (2017)
Au/GR–CS	2–935	0.35	0.347	Zhang et al. (2014)
Hb/AuNPs/carbon aerogel/ILs	5–950	2	–	Peng et al. (2015)
MWCNT@Hb/Nf	50–500	2.4	0.0283	Senthil Kumar et al. (2012)
Nanostructured tricobalt tetraoxide	0.1–50	0.145	0.0246	Barkaoui et al. (2015)
Chitosan-Prussian blue-graphene	25–3200	10	0.0587	Zhong et al. (2012)
Graphene-CS/PB	10–400	0.213	0.816	Yang et al. (2012)
CuO NWs/3D-Cu foam	1–1000	0.98	8.87	This work

investigated (Fig. S1). In this regard, the current response was recorded with the injection of 400 μM H_2O_2 at −0.2, −0.3, −0.4, and −0.5 V. It can be seen that the current response at −0.4 V possesses the highest value of the current response, implying this applied potential can produce better performance for CuO NWs/3D-Cu foam electrode towards H_2O_2 reduction. In another concern, the effect of pH on the response of the CuO NWs/3D-Cu foam electrode for H_2O_2 detection was also studied by amperometry. The influence of pH was tested in different PBS solutions with pH of 6.5, 7.0, 7.4, 8, and 8.5. Fig. S2 shows the change of current response against pH value under constant H_2O_2 concentration of 400 μM. As a

result, the highest current response is achieved at pH of 7.4. Therefore, pH of 7.4 was used for H_2O_2 detection in this research. For further comparing catalytic activity of different electrodes, a working potential of −0.4 V was applied for studying their amperometric response towards H_2O_2 reduction. It was found that the electrochemical behaviors of the CuO NWs/3D-Cu foam electrode displays the highest steady state of current density with successive addition of 400 μM H_2O_2 in 0.1 M PBS solution (Fig. 7A), further confirming the superior catalytic performance of the CuO NWs/3D-Cu foam electrode compared to two other electrodes. In addition, according to the successive injection of H_2O_2, the CuO NWs/3D-Cu foam electrode reaches the steady state within 5 s, implying its rapid response. Fig. 7B shows step-like amperometric current response against the successive addition of different H_2O_2 concentrations at the applied potential of −0.4 V. It can be seen the increase of current intensity is consistent with the increase of the injected H_2O_2 concentration. The corresponding calibration plot is presented in Fig. 7C, which clearly indicates good corresponding sensitivity, wide linear response range, and low LOD (S/N = 3). In this context, the CuO NWs/3D-Cu foam electrode shows the high sensitivity of 8.87 μA/(μM ṡ cm^2) and low LOD of 0.98 μM, along with a wide linear detection range of 1 μM–1 mM towards H_2O_2 detection. Meanwhile, the amperometric response of the CuOH NWs/3D-Cu foam electrode (Fig. S3) towards H_2O_2 detection displays a shorter detection range (10 μM–1.095 mM), higher LOD (6.7 μM), and lower sensitivity (3.3 - μA/(μM ṡ cm^2)) than those of the CuO NWs/3D-Cu foam electrode. A comparison of performance between the CuO NWs/3D-Cu foam electrode with recently reported non-enzymatic H_2O_2 sensors is shown in Table 1, which clearly evidences that the CuO NWs/3D-Cu foam electrode possesses superior performance to the reported sensors in terms of low LOD, high sensitivity, and wide detection range; therefore, it is highly promising for the detection of H_2O_2 concentration in the practical analysis.

In another regard, to evaluate whether the proposed CuO NWs/3D-Cu foam sensor is suitable for practical sensing application or not, the selectivity test was carried out. From Fig. 7D, it can be seen that there is a large response of current density by the first addition of 400 μM H_2O_2. Whereas, the subsequent additions of 0.05 mM urea, 0.05 mM dopamine (DA), 0.1 mM ascorbic acid (AA), 0.1 mM uric acid (UA), and 0.1 mM KCl do not produce any noticeable change of current intensity. A final addition of 400 μM H_2O_2 also provides relative current response compared to the first H_2O_2 addition. These achieved results inform that the CuO NWs/3D-Cu foam

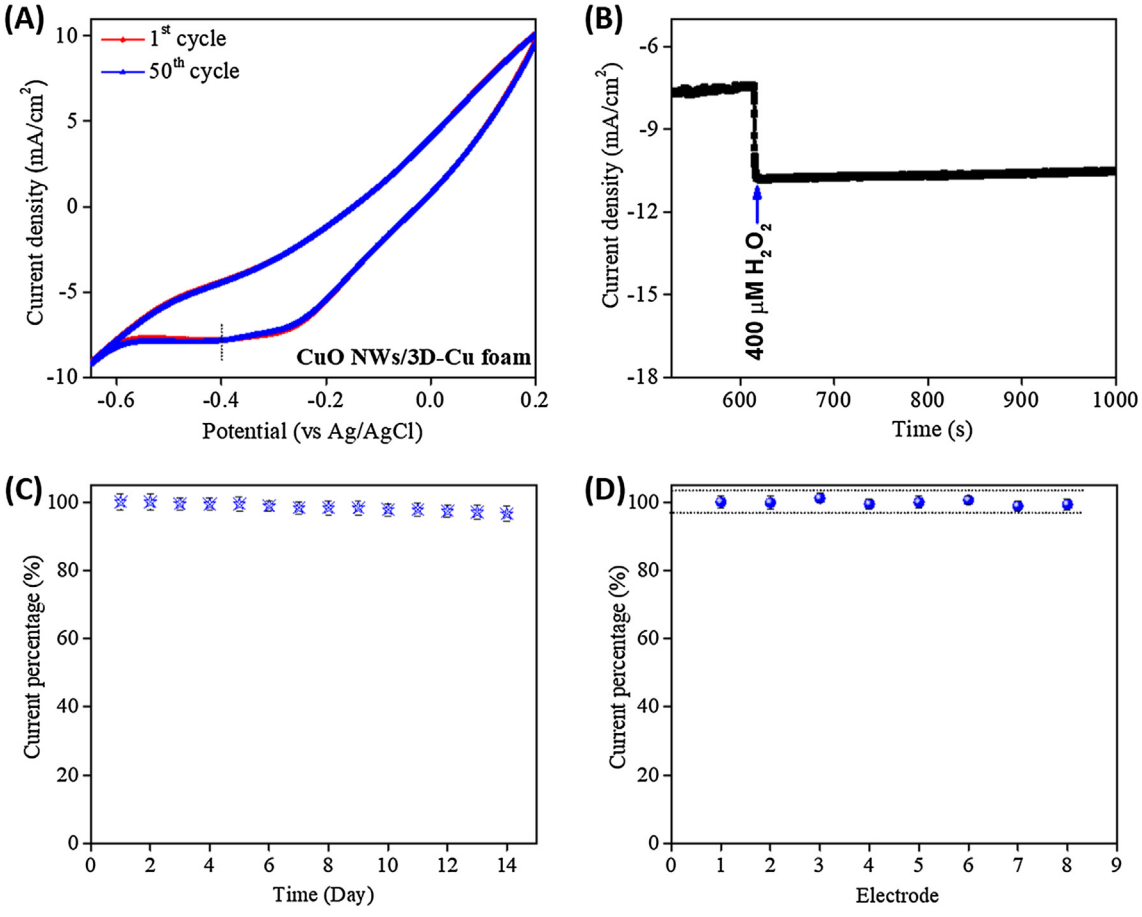

Fig. 8 (A) CV curves for long-term cycling time of the CuO NWs/3D-Cu foam electrode with presence of 1 mM H_2O_2 in 0.1 M PBS solution; (B) Durability of the CuO NWs/3D-Cu foam electrode after long term amperometric measurement at an applied potential of −0.4 V; (C) The store stability of the CuO NWs/3D-Cu foam electrode; (D) Reproducibility of the CuO NWs/3D-Cu foam electrode towards H_2O_2 detection.

Table 2 Detection of H_2O_2 in real samples using the CuO NWs/3D-Cu foam electrode.

Sample of blood serum spiked PBS solution	H_2O_2 added (μM)	H_2O_2 found (μM)	RSD (%)	Recovery (%)
1	200	198.5	3.11	99.2
2	400	394.9	4.28	98.7
3	800	795.7	3.55	99.5

electrode possesses good selectivity for H_2O_2 determination in the presence of other common interferents.

The stability, durability, and reproducibility of the developed CuO NWs/3D-Cu foam sensor were also evaluated. For investigating the stability of the CuO NWs/3D-Cu foam sensor, many CV cycles were measured in 1 mM H_2O_2 containing 0.1 M PBS solution (Fig. 8A). It can be seen that the CV curve of the material at first cycle and after 50th cycle does not show any noticeable change, implying its good stability for long-term working period. The amperometric current response with an addition of 400 μM H_2O_2 also indicates that the steady state of current density still remains 96.9% of original value after around 400 s, implying good durability of such electrode (Fig. 8B). In addition, the storage stability of the developed sensor was investigated by evaluating the amperometric current response for H_2O_2 reduction (400 μM H_2O_2) after two weeks (Fig. 8C). It is found that the current response achieved at 14th day decreases by 3.5% as compared to the 1st day. Furthermore, eight different electrodes were also used to evaluate the reproducibility of the CuO NWs/3D-Cu foam (Fig. 8D). The current response of seven following electrodes varies from 98.8 to 101.1% as compared to the result of the first electrode, suggesting impressive reproducibility of the synthesized CuO NWs/3D-Cu foam electrode for H_2O_2 detection.

To demonstrate the practical possibility of the CuO NWs/3D-Cu foam electrode, the blood serum (200 μL) spiked PBS solutions containing different known H_2O_2 concentrations (200, 400, 800 μL) were prepared. The H_2O_2 concentration in these samples was detected using amperometric measurement. The obtained results show the respectable RSD% of 3.11–4.28% and good recovery of 98.7–99.5% towards H_2O_2 detection, as summarized in Table 2. These suggest that the developed CuO NWs/3D-Cu foam-based sensor may be efficiently applied for H_2O_2 detection in practical analysis applications.

4. Conclusion

An interesting hierarchical nanomaterial of the vertical CuO NWs arrays on 3D-Cu foam was successfully fabricated to apply for non-enzymatic H_2O_2 sensor. The CuO NWs/3D-Cu foam electrode exhibited wide linear detection range of 1 μM-1 mM, high sensitivity of 8.87 μA/(μM ŝ cm^2), low LOD of 0.98 μM, fast response of 5 s, good reproducibility, and satisfactory selectivity for H_2O_2 detection in 0.1 M PBS solution. The cost-effective synthesis procedure and the outstanding catalytic performance suggest that the CuO NWs/3D-Cu foam material may be promising for non-enzymatic H_2O_2 sensing in practical analysis applications.

Acknowledgments

The authors acknowledge support from the fund of Duy Tan University in Da Nang city and Ton Duc Thang University in Ho Chi Minh city, Viet Nam. This research is funded by Vietnam National Foundation for Science and Technology Development (NAFOSTED) under grant number 107.01-2017.22.

Appendix A. Supplementary material

Supplementary data to this article can be found online at https://doi.org/10.1016/j.arabjc.2019.04.002.

References

Al-Hardan, N.H., Hamid, M.A.A., Shamsudin, R., Othman, N.K., Kar Keng, L., 2016. Amperometric non-enzymatic hydrogen peroxide sensor based on aligned zinc oxide nanorods. Sensors 16. https://doi.org/10.3390/s16071004.

ALOthman, Z.A., 2012. A review fundamental aspects of silicate mesoporous materials. Materials 5, 2874–2902. https://doi.org/10.3390/ma5122874.

Baghayeri, M., Rouhi, M., Lakouraj, M.M., Amiri-Aref, M., 2017. Bioelectrocatalysis of hydrogen peroxide based on immobilized hemoglobin onto glassy carbon electrode modified with magnetic poly(indole-co-thiophene) nanocomposite. J. Electroanal. Chem. 784, 69–76. https://doi.org/10.1016/j.jelechem.2016.12.006.

Barkaoui, S., Haddaoui, M., Dhaouadi, H., Raouafi, N., Touati, F., 2015. Hydrothermal synthesis of urchin-like Co < inf > 3 < / inf > O < inf > 4 < /inf > nanostructures and their electrochemical sensing performance of H < inf > 2 < /inf > O < inf > 2 < /inf >. J. Solid State Chem. 228, 226–231. https://doi.org/10.1016/j.jssc.2015.04.043.

Batchelor-McAuley, C., Du, Y., Wildgoose, G.G., Compton, R.G., 2008. The use of copper(II) oxide nanorod bundles for the non-enzymatic voltammetric sensing of carbohydrates and hydrogen peroxide. Sensor. Actuat. B-Chem. 135, 230–235. https://doi.org/10.1016/j.snb.2008.08.006.

Chandra Rath, P., Patra, J., Saikia, D., Mishra, M., Chang, J.K., Kao, H.M., 2016. Highly enhanced electrochemical performance of ultrafine CuO nanoparticles confined in ordered mesoporous carbons as anode materials for sodium-ion batteries. J. Mater. Chem. A 4, 14222–14233. https://doi.org/10.1039/c6ta05238j.

Chen, W., Chen, J., Feng, Y.-B., Hong, L., Chen, Q.-Y., Wu, L.-F., Lin, X.-H., Xia, X.-H., 2012. Peroxidase-like activity of water-soluble cupric oxide nanoparticles and its analytical application for detection of hydrogen peroxide and glucose. Analyst 137, 1706–1712. https://doi.org/10.1039/C2AN35072F.

Chen, W., Cai, S., Ren, Q.Q., Wen, W., Di Zhao, Y., 2012. Recent advances in electrochemical sensing for hydrogen peroxide: A review. Analyst 137, 49–58. https://doi.org/10.1039/c1an15738h.

Chen, S., Yuan, R., Chai, Y., Hu, F., 2013. Electrochemical sensing of hydrogen peroxide using metal nanoparticles: A review. Microchim. Acta. 180, 15–32. https://doi.org/10.1007/s00604-012-0904-4.

Erande, M.B., Late, D.J., 2016. Humidity and H $_{2\,O}$ 2 sensing behavior of Te nanowires. Adv. Device Mater. 2, 8–14. https://doi.org/10.1080/20550308.2016.1220148.

Etefagh, R., Azhir, E., Shahtahmasebi, N., 2013. Synthesis of CuO nanoparticles and fabrication of nanostructural layer biosensors for detecting Aspergillus niger fungi. Sci. Iran. 20, 1055–1058. https://doi.org/10.1016/j.scient.2013.05.015.

Evans, S.A.G., Elliott, J.M., Andrews, L.M., Bartlett, P.N., Doyle, P. J., Denuault, G., 2002. Detection of hydrogen peroxide at

mesoporous platinum microelectrodes. Anal. Chem. 74, 1322–1326. https://doi.org/10.1021/ac011052p.

Gimeno, P., Bousquet, C., Lassu, N., Maggio, A.F., Civade, C., Brenier, C., Lempereur, L., 2015. High-performance liquid chromatography method for the determination of hydrogen peroxide present or released in teeth bleaching kits and hair cosmetic products. J. Pharm. Biomed. Anal. 107, 386–393. https://doi.org/10.1016/j.jpba.2015.01.018.

Iivonen, T., Hämäläinen, J., Marchand, B., Mizohata, K., Mattinen, M., Popov, G., Kim, J., Fischer, R.A., Leskelä, M., 2016. Low-temperature atomic layer deposition of copper(II) oxide thin films. J. Vac. Sci. Technol. 34, 01A109. https://doi.org/10.1116/1.4933089.

Jia, B., Qin, M., Zhang, Z., Cao, Z., Wu, H., Chen, P., Zhang, L., Lu, X., Qu, X., 2016. The formation of CuO porous mesocrystal ellipsoids via tuning the oriented attachment mechanism. CrystEngComm. 18, 1376–1383. https://doi.org/10.1039/C5CE02249E.

Jin, Z., Liu, C., Qi, K., Cui, X., 2017. Photo-reduced Cu/CuO nanoclusters on TiO_2 nanotube arrays as highly efficient and reusable catalyst. Sci. Rep. 7, 1–9. https://doi.org/10.1038/srep39695.

Kuang, M., Li, T.T., Chen, H., Zhang, S.M., Zhang, L.L., Zhang, Y. X., 2015. Hierarchical $Cu_2O/CuO/Co_3O_4$ core-shell nanowires: synthesis and electrochemical properties. Nanotechnology 26, 304002. https://doi.org/10.1088/0957-4484/26/30/304002.

Li, Y., Cao, D., Liu, Y., Liu, R., Yang, F., Yin, J., Wang, G., 2012. CuO nanosheets grown on cupper foil as the catalyst for H_2O_2 electroreduction in alkaline medium. Int. J. Hydrogen Energy. 37, 13611–13615. https://doi.org/10.1016/j.ijhydene.2012.01.038.

Li, Z., Chen, Y., Xin, Y., Zhang, Z., 2015. Sensitive electrochemical nonenzymatic glucose sensing based on anodized CuO nanowires on three-dimensional porous copper foam. Sci. Rep. 5, 16115. https://doi.org/10.1038/srep16115.

Li, X., Liu, X., Wang, W., Li, L., Lu, X., 2014. High loading Pt nanoparticles on functionalization of carbon nanotubes for fabricating nonenzyme hydrogen peroxide sensor. Biosens. Bioelectron. 59, 221–226. https://doi.org/10.1016/j.bios.2014.03.046.

Li, Y., Zhang, J.J., Xuan, J., Jiang, L.P., Zhu, J.J., 2010. Fabrication of a novel nonenzymatic hydrogen peroxide sensor based on Se/Pt nanocomposites. Electrochem. Commun. 12, 777–780. https://doi.org/10.1016/j.elecom.2010.03.031.

Liu, J., 2017. Nanomaterial-based electrochemical hydrogen peroxide biosensor. Int. J. Biosens. Bioelectron. 2, 100–102. https://doi.org/10.15406/ijbsbe.2017.02.00027.

Liu, Y., Liao, L., Li, J., Pan, C., 2007. From copper nanocrystalline to CuO nanoneedle array: Synthesis, growth mechanism, and properties. J. Phys. Chem. C. 111, 5050–5056. https://doi.org/10.1021/jp069043d.

Marinho, H.S., Real, C., Cyrne, L., Soares, H., Antunes, F., 2014. Hydrogen peroxide sensing, signaling and regulation of transcription factors. Redox Biol. 2, 535–562. https://doi.org/10.1016/j.redox.2014.02.006.

Milton, N.G.N., 2004. Role of hydrogen peroxide in the aetiology of Alzheimer's disease: implication for treatment. Drugs Aging. 21, 81–100. https://doi.org/10.2165/00002512-200421020-00002.

Muralidharan, J.S.G., 2015. Amperometric sensing of hydrogen peroxide using glassy carbon electrode modified with copper nanoparticles. Mater. Res. Bull. 70, 315–320. https://doi.org/10.1016/j.materresbull.2015.04.058.

Nasirizadeh, N., Shekari, Z., Nazari, A., Tabatabaee, M., 2016. Fabrication of a novel electrochemical sensor for determination of hydrogen peroxide in different fruit juice samples. J. Food Drug Anal. 24, 72–82. https://doi.org/10.1016/j.jfda.2015.06.006.

Patra, S., Munichandraiah, N., 2009. Electrochemical reduction of hydrogen peroxide on stainless steel. J. Chem. Sci. 121, 675–683. https://doi.org/10.1007/s12039-009-0081-0.

Peng, L., Dong, S., Li, N., Suo, G., Huang, T., 2015. Construction of a biocompatible system of hemoglobin based on AuNPs-carbon aerogel and ionic liquid for amperometric biosensor. Sensor. Actuat. B-Chem. 210, 418–424. https://doi.org/10.1016/j.snb.2014.12.122.

Plauck, A., Stangland, E.E., Dumesic, J.A., Mavrikakis, M., 2016. Active sites and mechanisms for H_2O_2 decomposition over Pd catalysts. Proc. Natl. Acad. Sci. USA 113, E1973–E1982. https://doi.org/10.1073/pnas.1602172113.

Ryoo, D., Xu, X., Li, Y., Tang, J.A., Zhang, J., Van Zijl, P.C.M., Liu, G., 2017. Detection and quantification of hydrogen peroxide in aqueous solutions using chemical exchange saturation transfer. Anal. Chem. 89, 7758–7764. https://doi.org/10.1021/acs.analchem.7b01763.

Senthil Kumar, A., Gayathri, P., Barathi, P., Vijayaraghavan, R., 2012. Improved electric wiring of hemoglobin with impure-multi-walled carbon nanotube/nafion modified glassy carbon electrode and its highly selective hydrogen peroxide biosensing. J. Phys. Chem. C. 116, 23692–23703. https://doi.org/10.1021/jp3064933.

Shao, Y., Wang, J., Wu, H., Liu, J., Aksay, I.A., Lin, Y., 2010. Graphene based electrochemical sensors and biosensors : A review. Electronalysis 22, 1027–1036. https://doi.org/10.1002/elan.200900571.

Shiang, Y.C., Huang, C.C., Chang, H.T., 2009. Gold nanodot-based luminescent sensor for the detection of hydrogen peroxide and glucose. Chem. Commun., 3437–3439 https://doi.org/10.1039/b901916b.

Shichiri, M., 2014. The role of lipid peroxidation in neurological disorders. J. Clin. Biochem. Nutr. 54, 151–160. https://doi.org/10.3164/jcbn.14-10.

Singh, P., Nath, P., Arun, R.K., Mandal, S., Chanda, N., 2016. Novel synthesis of a mixed Cu/CuO-reduced graphene oxide nanocomposite with enhanced peroxidase-like catalytic activity for easy detection of glutathione in solution and using a paper strip. RSC Adv. 6, 92729–92738. https://doi.org/10.1039/c6ra20882g.

Sun, S., Sun, Y., Chen, A., Zhang, X., Yang, Z., 2015. Nanoporous copper oxide ribbon assembly of free-standing nanoneedles as biosensors for glucose. Analyst 140, 5205–5215. https://doi.org/10.1039/c5an00609k.

Tarvin, M., McCord, B., Mount, K., Miller, M.L., 2011. Analysis of hydrogen peroxide field samples by HPLC/FD and HPLC/ED in DC mode. Forensic Sci. Int. 209, 166–172. https://doi.org/10.1016/j.forsciint.2011.01.024.

Thetford, A., Hutchings, G.J., Taylor, S.H., Willock, D.J., 2010. The decomposition of H_2O_2 over the components of Au/TiO_2 catalysts. P. Roy. Soc. A-Math. Phy. 467, 1885–1899. https://doi.org/10.1098/rspa.2010.0561.

Toghill, K.E., 2014. Electrochemical non-enzymatic glucose sensors: a perspective and an evaluation. Int. J. Electrochem. Sci. 5 (2010), 1246–1301.

Wang, H., Guan, R., Fan, C., Zhu, D., Li, G., 2002. A hydrogen peroxide biosensor based on the bioelectrocatalysis of hemoglobin incorporated in a kieselgubr film. Sensor. Actuat. B-Chem. 84, 214–218. https://doi.org/10.1016/S0925-4005(02)00027-8.

Wang, Y., Lü, Y., Zhan, W., Xie, Z., Kuang, Q., Zheng, L., 2015. Synthesis of porous Cu_2O/CuO cages using Cu-based metal-organic frameworks as templates and their gas-sensing properties. J. Mater. Chem. A 3, 12796–12803. https://doi.org/10.1039/c5ta01108f.

Xing, M., Xu, W., Dong, C., Zhou, Y., Zhang, J., Yin, Y., 2018. Metal sulfides as excellent co-catalysts for H_2O_2 decomposition in advanced oxidation processes. Chem 4, 1359–1372. https://doi.org/10.1016/j.chempr.2018.03.002.

Xu, B., Ye, M.L., Yu, Y.X., De Zhang, W., 2010. A highly sensitive hydrogen peroxide amperometric sensor based on MnO_2-modified vertically aligned multiwalled carbon nanotubes. Anal. Chim. Acta. 674, 20–26. https://doi.org/10.1016/j.aca.2010.06.004.

Yang, S., Li, G., Wang, D., Qiao, Z., Qu, L., 2017. Synthesis of nanoneedle-like copper oxide on N-doped reduced graphene oxide: A three-dimensional hybrid for nonenzymatic glucose sensor.

Sensor. Actuat. B-Chem. 238, 588–595. https://doi.org/10.1016/j.snb.2016.07.105.

Yang, J.H., Myoung, N., Hong, H.G., 2012. Facile and controllable synthesis of Prussian blue on chitosan- functionalized graphene nanosheets for the electrochemical detection of hydrogen peroxide. Electrochim. Acta. 81, 37–43. https://doi.org/10.1016/j.electacta.2012.07.038.

Zhang, L., Yuan, F., Zhang, X., Yang, L., 2011. Facile synthesis of flower like copper oxide and their application to hydrogen peroxide and nitrite sensing. Chem. Cent. J. 5, 1–9. https://doi.org/10.1186/1752-153X-5-75.

Zhang, L., Han, G., Liu, Y., Tang, J., Tang, W., 2014. Immobilizing haemoglobin on gold/graphene-chitosan nanocomposite as efficient hydrogen peroxide biosensor. Sensor. Actuat. B-Chem. 197, 164–171. https://doi.org/10.1016/j.snb.2014.02.077.

Zhang, L., Ye, C., Li, X., Ding, Y., Liang, H., Zhao, G., Wang, Y., 2018. A CuNi/C nanosheet array based on a metal–organic framework derivate as a supersensitive non-enzymatic glucose sensor. Nano-Micro Lett. 10, 28. https://doi.org/10.1007/s40820-017-0178-9.

Zhao, B., Liu, Z., Liu, Z., Liu, G., Li, Z., Wang, J., Dong, X., 2009. Silver microspheres for application as hydrogen peroxide sensor. Electrochem. Commun. 11, 1707–1710. https://doi.org/10.1016/j.elecom.2009.06.035.

Zhong, X., Yuan, R., Chai, Y.Q., 2012. Synthesis of chitosan-Prussian blue-graphene composite nanosheets for electrochemical detection of glucose based on pseudobienzyme channeling. Sensor. Actuat. B-Chem. 162, 334–340. https://doi.org/10.1016/j.snb.2011.12.091.